

pubs.acs.org/JACS Article

# Characterization by ENDOR Spectroscopy of the Iron—Alkyl Bond in a Synthetic Counterpart of Organometallic Intermediates in Radical SAM Enzymes

Madeline B. Ho, Richard J. Jodts, Youngsuk Kim, Alex McSkimming, Daniel L. M. Suess,\* and Brian M. Hoffman\*



Cite This: J. Am. Chem. Soc. 2022, 144, 17642-17650



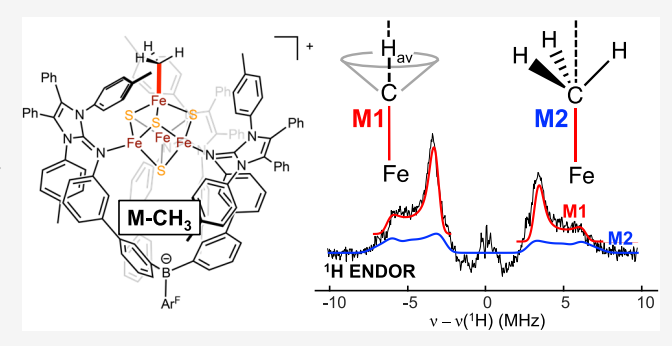
**ACCESS** I

III Metrics & More

Article Recommendations

s Supporting Information

**ABSTRACT:** Members of the radical S-adenosyl-L-methionine (SAM) enzyme superfamily initiate a broad spectrum of radical transformations through reductive cleavage of SAM by a [4Fe–4S]<sup>1+</sup> cluster it coordinates to generate the reactive S'-deoxyadenosyl radical (S'-dAdo $^{\bullet}$ ). However, S'-dAdo $^{\bullet}$  is not directly liberated for reaction and instead binds to the unique Fe of the cluster to create the catalytically competent S=1/2 organometallic intermediate  $\Omega$ . An alternative mode of reductive SAM cleavage, especially seen photochemically, instead liberates CH<sub>3</sub> $^{\bullet}$ , which forms the analogous S=1/2 organometallic intermediate with an Fe–CH<sub>3</sub> bond,  $\Omega_{\rm M}$ . The presence of a covalent Fe–C bond in both structures was established by the



ENDOR observation of  $^{13}C$  and  $^{1}H$  hyperfine couplings to the alkyl groups that show isotropic components indicative of Fe–C bond covalency. The synthetic  $[Fe_4S_4]^{3+}$ –CH<sub>3</sub> cluster, M-CH<sub>3</sub>, is a crystallographically characterized analogue to  $\Omega_M$  that exhibits the same  $[Fe_4S_4]^{3+}$  cluster state as  $\Omega$  and  $\Omega_{M}$ , and thus an analysis of its spectroscopic properties—and comparison with those of  $\Omega$  and  $\Omega_M$ —can be grounded in its crystal structure. We report cryogenic (2 K) EPR and  $^{13}C/^{1/2}H$  ENDOR measurements on isotopically labeled M-CH<sub>3</sub>. At low temperatures, the complex exhibits EPR spectra from two distinct conformers/subpopulations. ENDOR shows that at 2 K, one contains a static methyl, but in the other, the methyl undergoes rapid tunneling/hopping rotation about the Fe–CH<sub>3</sub> bond. This generates an averaged hyperfine coupling tensor whose analysis requires an extended treatment of rotational averaging. The methyl group  $^{13}C/^{1/2}H$  hyperfine couplings are compared with the corresponding values for  $\Omega$  and  $\Omega_M$ .

### ■ INTRODUCTION

Radical S-adenosyl-L-methionine (RS) enzymes, a superfamily with over  $5 \times 10^5$  members spanning all kingdoms of life, initiate a broad spectrum of radical transformations through use of S-adenosyl-L-methionine (SAM) and an [Fe<sub>4</sub>S<sub>4</sub>] cluster to liberate the reactive 5'-deoxyadenosyl radical (5'-dAdo\*) for H-atom abstraction.<sup>1,2</sup> SAM first binds to the [Fe<sub>4</sub>S<sub>4</sub>]<sup>1+</sup> cluster through its methionyl amino acid moiety, 3-6 and, for decades, it was believed that reductive cleavage of the SAM sulfonium by electron transfer from the cluster directly liberates the  $5'dAdo^{\bullet}$  radical for reaction with substrate.  $^{7-10}$  The RS mechanism underwent a paradigm shift when it was discovered that across the superfamily, 5'-dAdo formed by cleavage of the S-C5' bond of SAM first binds to the unique Fe of the cluster to create the catalytically competent organometallic intermediate  $\Omega$  (Figure 1); 5'-dAdo $^{\bullet}$  is only liberated for reaction with the substrate upon homolytic cleavage of the Fe-C5' bond of  $\Omega$ . Subsequent studies showed an alternative mode of reductive SAM cleavage, especially seen photochemically, in which reductive homolytic cleavage of the SAM methyl-sulfonium bond generates a CH<sub>3</sub> that reacts to form an analogous intermediate,  $\Omega_{\rm M}$ , in which the unique Fe forms an organometallic Fe–CH<sub>3</sub> bond, Figure 1. <sup>15</sup> Both intermediates were established by EPR and ENDOR spectroscopies to contain an [Fe<sub>4</sub>S<sub>4</sub>]<sup>3+</sup>—alkyl cluster. The S=1/2 spin of each was shown to reside on an [Fe<sub>4</sub>S<sub>4</sub>]<sup>3+</sup> cluster by its axial *g*-tensor with average *g*-value,  $g_{\rm iso}>2$ , and  $\Omega$  furthermore was shown to exhibit the large <sup>57</sup>Fe hyperfine couplings associated with such a cluster. <sup>12</sup> The presence of a covalent Fe–C bond in each was established by the observation of <sup>13</sup>C and <sup>1</sup>H hyperfine couplings to the alkyl that show isotropic components indicative of Fe–C covalency. <sup>11,12</sup>

Synthetic [Fe<sub>4</sub>S<sub>4</sub>]-alkyl clusters have been prepared to better understand the properties of these enzymatic

Received: July 7, 2022

Published: September 15, 2022





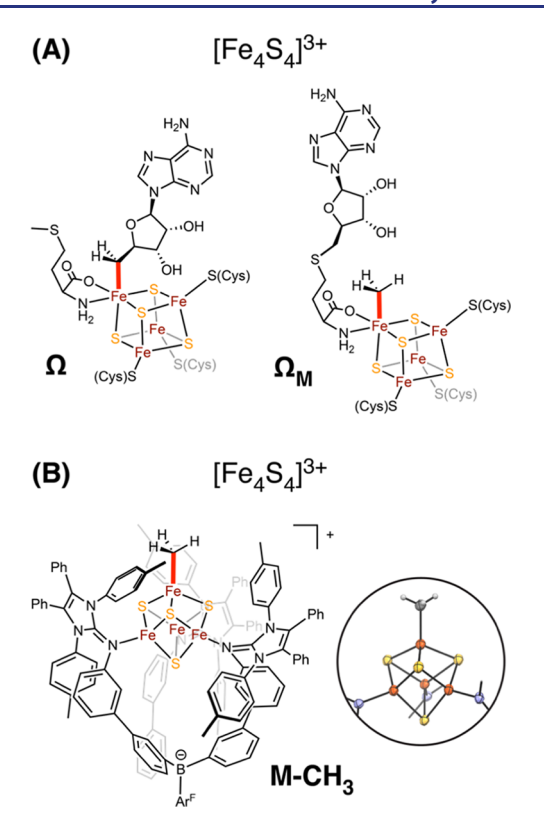


Figure 1. Proposed structures of  $\Omega$  and  $\Omega_M$  (A) and crystallographically determined structure of M-CH<sub>3</sub> (B).

intermediates.  $^{16-18}$  Of the synthetic  $[Fe_4S_4]$ -alkyl clusters reported to date, cluster M-CH<sub>3</sub> (Figure 1B), a structurally characterized analogue to  $\Omega_{\rm M}$  (Figure 1), is the only one with the same core charge state as that in  $\Omega$  and  $\Omega_{\rm M}$ :  $[{\rm Fe_4S_4}]^{3+}$ . 18 Like  $\Omega$  and  $\Omega_{\rm M}$ , it adopts an S=1/2 ground state with average g-value,  $g_{\rm iso}$ , >2. <sup>18</sup> Importantly, **M-CH**<sub>3</sub> has been crystallographically characterized, and thus its composition, connectivity, and bond lengths are known without ambiguity. As such, analysis of its spectroscopic properties—and comparison with those of  $\Omega$  and  $\Omega_{\mathrm{M}}$ —can be grounded in its crystal structure. We report here cryogenic EPR and <sup>13</sup>C/<sup>1/2</sup>H ENDOR measurements on isotopically labeled M-CH<sub>3</sub> and compare them with the corresponding measurements on  $\Omega$ and  $\Omega_{\rm M}$ .

#### MATERIALS AND METHODS

Sample Preparation. The previously reported cluster,  $[(L^{B}(NIm)_{3})Fe_{4}S_{4}CH_{3}][B(C_{6}F_{5})_{4}]^{1}$  (M-CH<sub>3</sub>), was prepared as described. The isotopologues M-<sup>13</sup>CH<sub>3</sub> and M-C(<sup>2</sup>H)<sub>3</sub> were prepared in an identical manner except with the methyl groups sourced from (13CH<sub>3</sub>)<sub>2</sub>Mg and (C(2H)<sub>3</sub>)<sub>2</sub>Mg, respectively, instead of natural abundance (CH<sub>3</sub>)<sub>2</sub>Mg. Samples were prepared in an N<sub>2</sub>-filled glovebox as 1 mM solutions, loaded into custom quartz Q-band tubes, frozen in LN2, and kept under LN2 until spectroscopic characterization.

EPR and ENDOR Measurements. All CW (continuous wave) Xband EPR measurements were performed on a Bruker ESP-300 spectrometer with a liquid helium flow Oxford Instruments ESR-900 cryostat. The 35 GHz CW EPR and ENDOR spectra were recorded on a modified Varian E-110 spectrometer equipped with a helium immersion dewar.<sup>19</sup> As the X- and Q-band spectra are collected in different spectrometers at different frequencies and in different detection modes—unsaturated absorption mode at X-band with derivative display through field modulation, rapid-passage dispersion

mode with absorption-display at Q-band—the lineshapes and g-values determined by EPR simulations differ very slightly (third significant figure in g-values) for the two types of spectra. This has no impact on the collection of 2D field-frequency patterns of ENDOR spectra collected across the Q-band EPR envelope, and in the text, g-values are only given to two significant figures. <sup>13</sup>C ENDOR used swept CW ENDOR. The <sup>1</sup>H CW ENDOR was collected using the field modulation-detected stochastic ENDOR sequence for better resolution of the features. Pulsed ENDOR measurements were collected at ~2 K, where electron spin relaxation is slow in both M-CH<sub>3</sub> conformers, on a spectrometer described previously, with SpinCore PulseBlaster ESR PRO 400 MHz digital word generator and Agilent Technologies Acquiris DP235 500 MS/s digitizer using SpecMan4EPR software. To For H pulsed ENDOR, a Mims pulse sequence  $[\pi/2-\tau-\pi/2-T_{RF}-\pi/2]$  was employed, in which  $\tau$  is the microwave pulse duration and T<sub>RF</sub> denotes the time interval in which the RF is applied. For <sup>1</sup>H pulsed ENDOR, a Davies pulse sequence  $[\pi - T_{RF} - \pi/$  $2-\tau-\pi$ ] was employed. Both EPR and ENDOR simulations were carried out with EasySpin using the pepper and salt functions, respectively.

Hyperfine Sign Determination. To obtain the signs of the measured hyperfine couplings (more precisely, the sign of  $A/g_N$  where  $g_N$  is the nuclear g-factor and is positive for  $^1H$  and  $^{13}C$  studied here), the Pulsed ENDOR SaTuration-REcovery (PESTRE) method was used at 35 GHz, as described in detail previously<sup>22</sup> and discussed

#### RESULTS

EPR of M-CH<sub>3</sub>. Figure 2 shows the temperature dependence of EPR spectra of M-CH<sub>3</sub>. At 40 K, M-CH<sub>3</sub> appears to

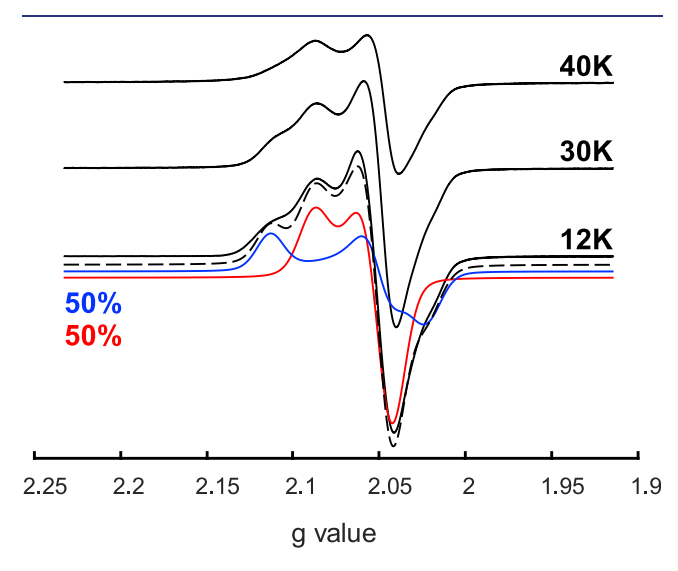
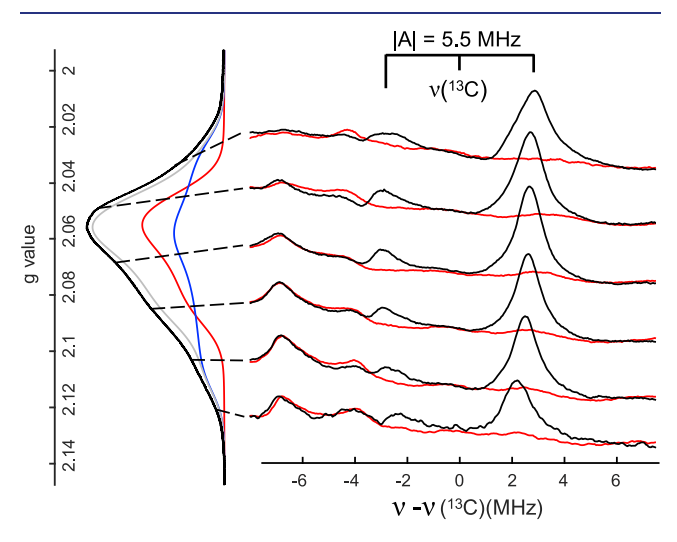


Figure 2. CW X-band EPR spectra of M-CH<sub>3</sub> in 3:1 DFB/toluene. Conditions: temperature 12, 30, and 40 K; 9.375 GHz microwave frequency; 10 G modulation amplitude; 320 ms time constant; 200  $\mu W$  microwave power. Simulation parameters: g = [2.088, 2.052,[2.042] (red), g = [2.113, 2.05, 2.022] (blue), sum (dashed).

give a somewhat poorly defined signal with an axial g-tensor characteristic of an  $[\text{Fe}_4\text{S}_4]^{3+}$  cluster,  $g_{\parallel} \approx 2.09 > g_{\perp} \approx 2.04 > 2$ ,  $g_{\text{iso}} = (g_{\parallel} + 2g_{\perp})/3 > 2$ . As the temperature is lowered, the poor resolution at 40 K improves, and by 12 K, the spectrum can be decomposed into well-defined contributions from two cluster conformers with comparable populations, one with  $g_{\parallel} \approx$ 2.09 that persists at higher temperatures, denoted M1-CH<sub>3</sub>, and a more-anisotropic signal with  $g_{\parallel} \approx 2.11$  from the second conformer, denoted M2-CH3. Figure S1 shows that the properties of the two conformers vary only slightly with

solvent but that the relative populations vary significantly. Rapid increases in spin relaxation with temperature restrict ENDOR measurements to cryogenic temperatures (and thus also to frozen solution). Whereas two states are observed by EPR of the frozen solution, the fluid-solution  $^1H$  NMR spectra of M-CH<sub>3</sub> recorded at T > 193 K show only a single set of resonances.  $^{18}$  This difference indicates that in fluid solution, the two conformers rapidly interconvert on the NMR timescale.

<sup>13</sup>C ENDOR. The signature feature of M-CH<sub>3</sub> is its organometallic Fe-CH<sub>3</sub> bond, and isotopic labeling of the methyl group has enabled the use of <sup>13</sup>C ENDOR to characterize this bond. The 2D field-frequency pattern of <sup>13</sup>C ENDOR spectra collected across the EPR envelope of M-<sup>13</sup>CH<sub>3</sub> is displayed in Figure 3. It shows a single <sup>13</sup>C



**Figure 3.** Q-band CW  $^{13}$ C ENDOR spectra (right) of M-( $^{13}$ C)H<sub>3</sub> (black), natural abundance M-CH<sub>3</sub> (red), and absorption-display EPR spectrum of M-CH<sub>3</sub> (left) and two-component simulations with parameters as in Figure 2. Spectra centered at  $^{13}$ C Larmor frequency. Feature centered at  $^{-5}$  MHz is  $^{14}$ N signal from the scorpionate ligand. ENDOR conditions: 2 K, 34.934 GHz microwave frequency for natural abundance sample, 35.01 GHz microwave frequency for  $^{13}$ C sample, 3.2 G modulation amplitude, 1.2  $\mu$ W MW power, forward-swept, 32 ms time constant, scan speed 3 MHz/s,  $^{10}$ -100 scans for each. The intensities of natural abundance spectra were scaled to the corresponding  $^{13}$ C spectra intensity by scaling the scorpionate  $^{14}$ N signal.

doublet with a near-isotropic splitting of magnitude, A = 5.5 MHz. As this signal is the summation of responses from the two conformers in comparable amounts, the observation of a single doublet at all fields indicates that the Fe–C bonding is essentially identical in both conformers. The presence of this isotropic <sup>13</sup>C hyperfine interaction establishes the covalency of the Fe–C bond, as also inferred from previous <sup>57</sup>Fe Mössbauer spectroscopic analysis. <sup>18</sup> The slight changes in apparent lineshape across the field can be attributed to an extremely small anisotropic component to the hyperfine couplings that manifests itself differently in the signals from the two conformers, in part, because of the difference in their g-values.

The sign of the <sup>13</sup>C hyperfine coupling is critical for connecting hyperfine values to bonding descriptions but is not given by conventional ENDOR measurements. To determine the hyperfine sign, we thus conducted Pulsed ENDOR SaTuration-REcovery, PESTRE measurements, Figure 4.<sup>22</sup>

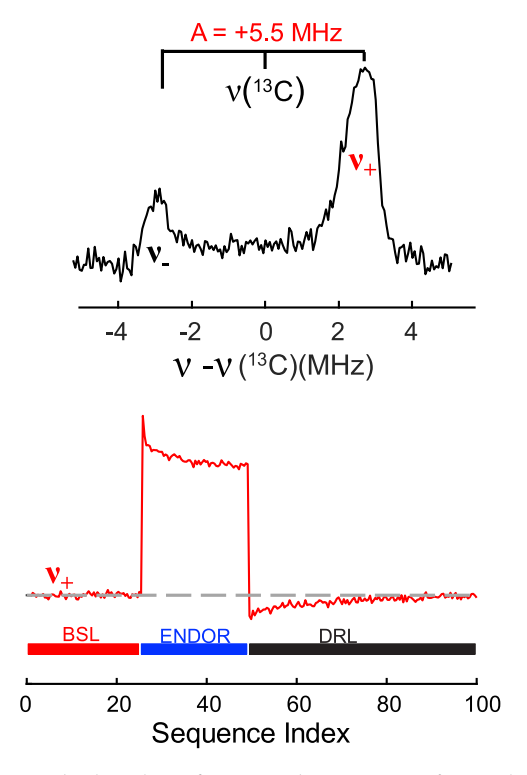


**Figure 4.** Absolute hyperfine sign determination for methyl  $^{13}\text{C}$  coupling at g=2.05. (Top) Baseline-corrected Q-band Davies pulsed  $^{13}\text{C}$  ENDOR. (Bottom)  $^{13}\text{C}$  PESTRE trace collected from the  $\nu_+$  branch of the  $^{13}\text{C}$  coupling. ENDOR conditions: 34.753 GHz microwave frequency,  $\pi=120$  ns,  $\tau=600$  ns,  $t_{\rm rf}=35~\mu{\rm s}$ , rf tail = 5  $\mu{\rm s}$ , repetition time = 50 ms, spectral resolution 256 points, temperature 2 K, PESTRE collected at rf frequency 15.8 MHz.

This protocol employs a multisequence of Davies ENDOR electron spin-echo pulse sequences. The first set of sequences is applied without applied RF and establishes a "baseline (BSL)" steady-state electron spin-echo response; each sequence in the second set incorporates an RF pulse at a chosen frequency (ENDOR); the response in the third set exhibits a dynamic reference level (DRL) whose offset from BSL is induced by relaxation effects that depend on the sign of the hyperfine coupling and that decays to BSL. The signs of the deviation of the DRL from the BSL (denoted DRL- $\delta$ ) at the  $\nu_+$  and  $\nu_-$  partners of a hyperfine doublet independently establish the sign of the hyperfine coupling.

The  $^{13}$ C ENDOR response from  $M^{-\hat{13}}$ CH<sub>3</sub> exhibits the well-resolved  $\nu_-/\nu_+$  doublet of Figure 3, and both branches have been probed with PESTRE. The weaker  $\nu_-$  peak does not give a clear PESTRE signature for sign assignment, but the clean observation of DRL- $\delta$  < 0 when probing  $\nu_+$  (Figure 4) unambiguously establishes that the  $^{13}$ C hyperfine coupling is positive: the essentially isotropic  $^{13}$ C hyperfine coupling thus has the positive value  $a_{\rm iso}(^{13}{\rm C}) = +5.5$  MHz. This coupling is caused by positive spin density on the methyl  $^{13}$ C, which arises because the spin-down unpaired electrons on the alkylated Fe center polarize the doubly occupied Fe–C  $\sigma$ -bond, inducing positive spin density at C (Scheme S1).

The conclusion that the methylated Fe center exhibits negative spin density is consistent with previous NMR analysis of M-CH<sub>3</sub>. The surprising absence of a distinct anisotropy to the <sup>13</sup>C coupling implies that the through-space dipole—dipole interaction with the down-spin electrons on the unique Fe, as modified by smaller contributions from the other Fe's, is

almost exactly offset by an oppositely signed anisotropic interaction with the positive (spin-up) local spin on C.

<sup>1,2</sup>H ENDOR Analysis of the M1-C( $^{1,2}$ H)<sub>3</sub> Conformer. In parallel, we carried out  $^{1,2}$ H ENDOR studies of M-CH<sub>3</sub> and its isotopologue, M-C( $^{2}$ H)<sub>3</sub>, at 2 K. Figure 5A shows the richly featured  $^{1}$ H ENDOR spectrum of M-CH<sub>3</sub> taken near the peak of the absorption-display EPR spectrum (g = 2.065), whose breadth corresponds to a maximum  $^{1}$ H hyperfine coupling of  $A \sim 15$  MHz. The  $^{1}$ H signals specifically associated with the Febound C( $^{1}$ H)<sub>3</sub> are absent in the spectrum of M-C( $^{2}$ H)<sub>3</sub> and

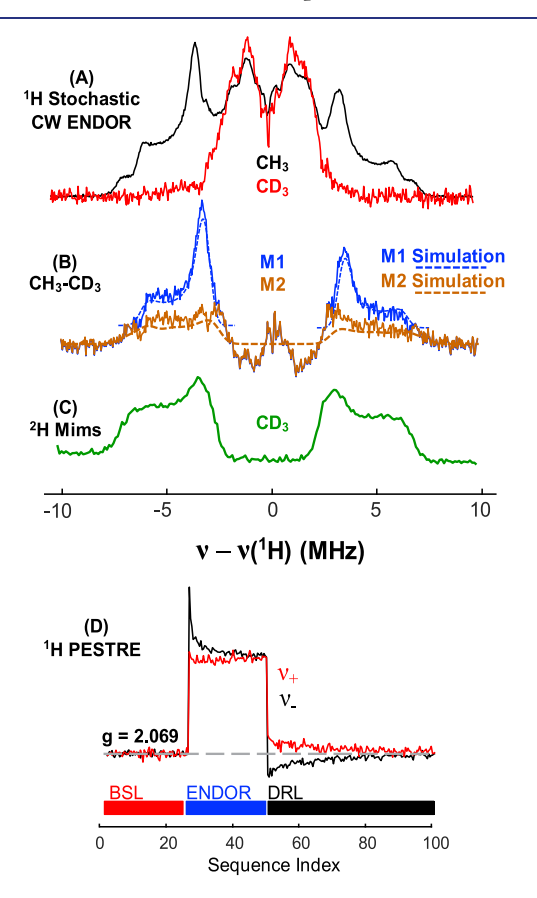
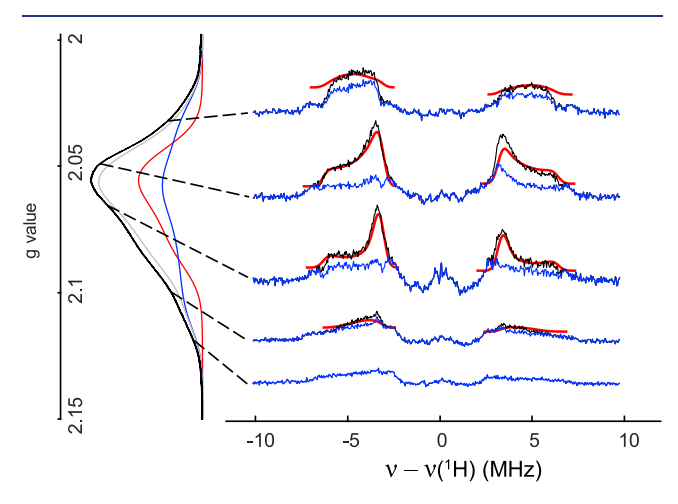


Figure 5. (A) Q-band stochastic <sup>1</sup>H ENDOR at field corresponding to g = 2.05 of M-CH<sub>3</sub> (black) and M-CD<sub>3</sub> (red), scaled to equalize the intensity of nonexchangeable proton couplings. (B) Spectrum upon subtraction of M-CD<sub>3</sub> from M-CH<sub>3</sub> partitioned into M1-CH<sub>3</sub> (blue) and M2-CH3 (gold) contributions. Simulation of M1-CH3 (blue, dashed) uses a single axial hyperfine tensor. M2-CH3 contribution obtained by subtracting M1 simulation from CH<sub>3</sub>-CD<sub>3</sub> difference spectrum. M2-CH<sub>3</sub> simulation discussed in text and described in Supporting Information. (C) Q-band Mims <sup>2</sup>H ENDOR spectra scaled to <sup>1</sup>H frequency by a factor  $g_N(^1H)/g_N(^2H) = 6.514$  at field corresponding to g = 2.05. (D) <sup>1</sup>H PESTRE trace collected at the  $\nu_{+}$  branch (red) and  $\nu_{-}$  branch (black) of the <sup>1</sup>H coupling at g = 2.07. <sup>1</sup>H stochastic ENDOR conditions: 2 K, ~35.1 GHz MW frequency, 3.2 G modulation amplitude, 1.2  $\mu$ W MW power, 2 s rf on, 2 s rf off, 0.5 s wait time, 150–1250 scans each. <sup>2</sup>H Mims ENDOR conditions: 2 K, microwave frequency 34.74 GHz,  $\pi = 100$  ns,  $\tau = 300$  ns,  $t_{\rm rf} = 60$  $\mu$ s, rf tail = 10  $\mu$ s, repetition time 50 ms, spectral resolution 256 points.  $^{1}$ H PESTRE conditions: 34.753 GHz microwave frequency,  $\pi$ = 120 ns,  $\tau$  = 600 ns,  $t_{\rm rf}$  = 35  $\mu$ s, rf tail = 5  $\mu$ s, repetition time = 50 ms, spectral resolution 256 points, temperature 2 K, PESTRE collected at rf frequency 47.67 and 54.55 MHz. M1-CH3 ENDOR simulation parameters: g = [2.091, 2.054, 2.042], where  $g_1 = g_{\parallel}$  corresponds to the z-direction in a conventional coordinate frame;  $A = \begin{bmatrix} -12.7 & -6.45 \end{bmatrix}$ -6.45], and  $[\alpha, \beta, \gamma] = [0, 55, 0]$ .

are better visualized by subtraction of the two spectra, Figure SB. These spectra are in turn complemented by the  $^2$ H Mims ENDOR signals introduced by deuterium substitution in **M**-C( $^2$ H)<sub>3</sub>, which match well with the methyl  $^1$ H signals upon scaling the  $^2$ H frequencies by the ratio of proton and deuteron nuclear *g*-factors,  $g_N(H)/g_N(D) = 6.518$ , given that the features of the  $^2$ H spectra are broadened by unresolved  $^2$ H quadrupole coupling (see Supporting Information), with the appearance of broadening enhanced by the presentation on the scaled frequency axis. This is illustrated in Figure SC for g = 2.065, while Figure S2 shows that the full 2D field-frequency pattern of  $^2$ H Mims spectra of **M**-C( $^2$ H)<sub>3</sub> mirrors the pattern of  $^1$ H spectra of **M**-C( $^1$ H)<sub>3</sub>, Figures 6 and S3.



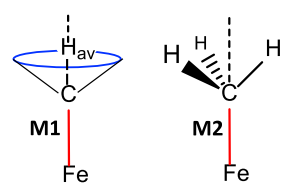
**Figure 6.** Subtraction of Q-band stochastic <sup>1</sup>H ENDOR spectra of **M**-CH<sub>3</sub> and **M**-CD<sub>3</sub> to give the methyl–proton spectrum (black), simulation of a single axial hyperfine tensor for **M**1-CH<sub>3</sub> (red), and result of subtracting simulation from CH<sub>3</sub>–CD<sub>3</sub> difference spectrum (blue) (right), along with the absorption-display EPR spectrum of M-CH<sub>3</sub> (left) with simulations as in Figure 3. <sup>1</sup>H stochastic ENDOR conditions: 2 K, ~35.1 GHz MW frequency, 3.2 G modulation amplitude, 1.2 μW MW power, 2 s rf on, 2 s rf off, 0.5 s wait time, 150–1250 scans each. ENDOR simulation parameters: g = [2.091, 2.054, 2.042], where  $g_1 = g_{\parallel}$  corresponds to the z-direction in a conventional coordinate frame;  $A = -[12.7 \ 6.45 \ 6.45]$ , and  $[\alpha, \beta, \gamma] = [0, 55, 0]$ ; the absolute sign is determined as described in text.

Figure 2 shows that the EPR signal of M-CH<sub>3</sub> is a sum of signals from two conformers, and consequently, the <sup>1</sup>H ENDOR spectra of M-CH<sub>3</sub> are a superposition of ENDOR responses from the two at fields where the EPR spectra overlap (Figures 5B, 6, and S3). M2-CH<sub>3</sub> alone contributes to the EPR and thus to both <sup>1</sup>H (Figures 6 and S3) and <sup>2</sup>H ENDOR spectra at the high- and low-field edges of the EPR spectrum because of the greater M2-CH<sub>3</sub> g-anisotropy.

Simulations of the cryogenic (2 K) 2D field-frequency pattern of orientation-dependent  $^{1}H$  ENDOR spectra collected across the M1-CH<sub>3</sub> portion of the EPR envelope, Figures 6 and S3, show that the three methyl protons of the M1-CH<sub>3</sub> conformer exhibit a well-defined joint, averaged  $^{1}H$  response characteristic of the frozen solution of a center with axial gtensor, and a single hyperfine-coupled proton with noncoaxial hyperfine tensor that is itself precisely axial.  $^{28,29}$  As discussed further below, this behavior at 2 K is most simply understood as arising from tunneling and/or hopping of the methyl protons through rotations of  $2\pi/3$  among the energetic minima of a three-fold symmetric potential surface that

rotationally averages the hyperfine tensor. This behavior of  $M1\text{-}CH_3$  is analogous to the tunneling/hopping averaging for H<sub>2</sub> in nonclassical Fe- and Co-H<sub>2</sub> complexes<sup>30,31</sup> and is captured in the cartoon of Scheme 1.

Scheme 1. Representation of Fe-CH<sub>3</sub> Behavior in the Rotationally Averaged M1 and Static M2 Conformers



The complete averaged <sup>1</sup>H hyperfine tensor derived above from simulations is  $A1(^{1}H)^{av} = -[12.7, 6.45, 6.45]$  MHz, with Euler angles defining the hyperfine tensor orientation relative to the *g*-tensor frame of  $[\alpha, \beta, \gamma] = [0, 55, 0]$ . The relative signs of the components are fixed by the simulations of the field dependence; the negative absolute sign of the components is obtained by use of the multisequence PESTRE protocol. This is shown in Figure 5D for a measurement at g = 2.065, with the RF set to a frequency near the maximum C(1H), ENDOR intensity of M1-CH3; PESTRE measurements at additional fields corresponding to the other principal g-values of M1-CH<sub>3</sub> give the same negative sign for the interaction, Figure S4, while PESTRE measurements described below show that the <sup>1</sup>H couplings for M2-CH3 likewise are negative. The observed averaged M1-CH<sub>3</sub> <sup>1</sup>H hyperfine tensor, A1(<sup>1</sup>H)<sup>av</sup>, thus can be decomposed into a negative isotropic coupling,  $a_{iso}^{av} = -8.5$ MHz, and a negative axial anisotropic tensor  $\mathbf{T}^{av} = [T_{\parallel}^{av}, T_{\perp}^{av},$  $T_{\perp}^{\text{av}}$ ] = -[4.2, -2.1, -2.1] MHz. The negative sign of the A(1H)av tensor of M1-CH3, in particular, that of the isotropic coupling, is in agreement with that implied by the negative paramagnetic shift of the methyl protons previously observed in VT-NMR. 18 To understand the negative sign, we note that the Fe-CH<sub>3</sub> protons are " $\beta$ " to Fe, and as a result, the isotropic contribution to the hyperfine coupling,  $a_{iso}^{av} = -8.5$ MHz can be attributed to spin transfer from the "down-spin" on Fe to the protons through hyperconjugation and/or through bond spin polarization from Fe through C to the coupled <sup>1</sup>H.

<sup>1</sup>H ENDOR of Conformation M2-CH<sub>3</sub>. For fields at which the EPR spectrum of M2-CH3 overlaps that of M1-CH3, subtraction of the <sup>1</sup>H ENDOR simulation of the single proton representing the rotationally averaged methyl protons of M1-CH<sub>3</sub> from the observed spectrum gives the <sup>1</sup>H ENDOR response of M2-CH<sub>3</sub>, as illustrated in Figure 5B. In addition, as noted, the M2-CH3 EPR signal, and thus its ENDOR signals, persist in both lower and higher fields because of its greater ganisotropy. Figures 6 and S5 show the resulting M2-CH<sub>3</sub> <sup>1</sup>H ENDOR spectra collected across the EPR envelope of this conformer. These signals are of low intensity and nearly featureless across the EPR envelope, with a maximum coupling that is somewhat larger than the M1-CH3 maximum and that remains roughly constant across the field at a value,  $A \sim -15$ MHz, Figures 6 and S5. The negative sign of A(<sup>1</sup>H) for this conformer is likewise established by PESTRE measurements at multiple fields and frequencies, Figures 4, S4, and S6.

The broad, low-intensity <sup>1</sup>H ENDOR responses of M2-CH<sub>3</sub> indicate that this methyl is essentially static, Scheme 1. For a static M2-CH<sub>3</sub>, the three methyl protons necessarily have

differently oriented hyperfine tensors and may well have different hyperfine components as the result of a hyperconjugative interaction with the Fe anchor and/or dipolar interactions with the other cluster Fe. Thus, they resonate over a different range of frequencies at each g-value of observation. Their signals neither track nor reinforce each other at fields across the EPR envelope, resulting in an essentially featureless signal whose total breadth varies little. For illustration, Figure S5 shows the 2D pattern of M2-CH3 spectra is well reproduced by summation of three tetrahedrally oriented methyl group <sup>1</sup>H hyperfine tensors with similar isotropic couplings ( $a_{iso} = -8 \leftrightarrow -10 \text{ MHz}$ ) and anisotropic coupling tensor components (average value of unique component, T2<sub>11</sub><sup>a</sup>  $\cong$  -5 MHz). The proton signals from conformer M2-CH<sub>3</sub> are substantially less intense than those of M1-CH3 despite the  $\sim$ 50/50 ratio of conformer populations in the simulation of the 12 K EPR spectrum (Figure 1) because of the M1-CH3 rotational averaging. The averaged M1 <sup>1</sup>H signal arises from three protons that resonate at the same frequency with every orientation of the Fe-C center relative to the external field (same hyperfine tensor components and orientation), and thus their contributions coherently add, unlike those of the M2 protons with their different tensor orientations.

Finally, why is methyl rotation stopped for conformer M2 but not M1? We speculate that in a frozen solution, the two conformers exhibit differential solvent access to the unique Fe site. Specifically, small differences thus introduced in the Fe-N, N-C(imidazole), and/or N-C(tolyl) torsion angles of the M2 conformer could yield large secondary structure changes in the scorpionate ligand that hinder the methyl rotation or bring solvent molecules near the methyl that have this effect. Presumably, the effects that quench M2 methyl rotation in the solid state at 2 K also slightly distort the cluster geometry, thereby changing the spin coupling among the Fe ions and/or individual site g-tensors sufficiently to slightly modify the observed g-values. An underlying solvent influence is supported by the observation that varying the solvent composition changes the relative occupancy of the two conformers (Figure S1). However, as we show below, the properties of the Fe-CH<sub>3</sub> bond are the same in the two conformers.

Rotational Averaging of the M1-C(1H)<sub>3</sub> Anisotropic Hyperfine Interactions. As presented above, the averaged orientation-selective <sup>1</sup>H ENDOR response from the three CH<sub>3</sub> protons of the M1-CH<sub>3</sub> conformer at 2 K is characteristic<sup>28,29</sup> of the frozen solution of a center with axial g-tensor and hyperfine coupling to a single proton whose hyperfine tensor is itself precisely axial but noncoaxial with the g-tensor; it is not the sum of distinct and differing individual signals from each of the three protons, as seen for M2-CH3. As visualized in Scheme 1 (left), at 2 K, the M1-CH<sub>3</sub> methyl group undergoes rapid rotation about the Fe-C bond through tunneling/ hopping on its three-fold symmetric ground-state potential energy surface, thereby averaging the M1-CH3 methyl group proton hyperfine tensors in behavior analogous to the tunneling/hopping of H<sub>2</sub> in a nonclassical trigonally symmetric Fe-H<sub>2</sub> complex.<sup>31</sup> The extensive literature discussing the dynamics of methyl group rotation includes numerous considerations of how such rotation can affect the <sup>1</sup>H ENDOR spectra of the methyl protons, 24-27,32,33 However, here we focus on the properties of the M-CH<sub>3</sub> complex and its organometallic Fe-C bond, and thus address the consequences of the rotational averaging on the <sup>1</sup>H hyperfine tensor of the M1 conformation. In most prior studies, the methyl group

under consideration is part of an organic radical whose EPR spectrum is without resolved *g*-anisotropy, while the hyperfine coupling is large and largely isotropic. To our knowledge, it has not been explicitly recognized that rotation does not merely average the coupling constants of the three methyl protons. When the methyl group is part of a paramagnetic center that exhibits well-resolved *g*- and hyperfine-anisotropy, an additional level of averaging is required to generate orientation-resolved ENDOR spectra in which the three methyl <sup>1</sup>H nuclei jointly give a 2D field-frequency pattern of ENDOR spectra that appears as though it were from a single <sup>1</sup>H with an averaged, anisotropic hyperfine tensor.

The three protons of a static methyl likely have hyperfine tensors with different component values, but must have differently oriented (noncolinear) anisotropic interaction tensors, and this is necessarily true for the H-atoms of the M1-CH<sub>3</sub> methyl. Thus, the observation of a single joint, orientation-selective <sup>1</sup>H ENDOR pattern requires not only that the three <sup>1</sup>H nuclei of the M1 methyl exhibit hyperfine tensors with the same components, whether intrinsically or through rotational averaging, but beyond that it also requires that rotational averaging of the single-site tensors themselves gives them a common averaged orientation. As discussed next, and in more detail in Supporting Information, this rotational averaging reorients the observed, averaged, joint hyperfine tensor, redefines its "symmetry" by making it precisely axial, and modifies the component values of the anisotropic interaction from those of the single-site tensors.

To understand the rotational averaging of a methyl proton hyperfine tensor, consider Figure 7A, which shows one of the

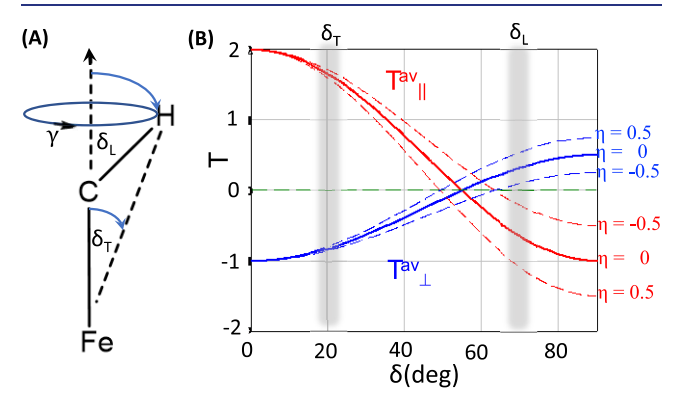


Figure 7. (A) Depiction of methyl Fe–C–H structure with angle  $\delta_T$ , the angle between the Fe–C bond/rotation axis and the dashed line, which represents the unique axis of through-space  $^1\mathrm{H}$  dipolar coupling to spin on Fe, and the angle  $\delta_L$  between the Fe–C bond and the C–H bond, along which lies the unique axis for  $^1\mathrm{H}$  anisotropic coupling to spin on C. (B) Plot of the axial anisotropic hyperfine parameters,  $T_{\parallel}^{\mathrm{av}}$ ,  $T_{\perp}^{\mathrm{av}}$ , obtained upon assumption of rapid rotation of the methyl about Fe–C (eq S3), for convenience normalized to a reference scaling factor (eq 1), T=+1 (positive spin density on Fe), and plotted as function of δ for several values of rhombicity parameter, η. For negative T (negative Fe spin density) and a corresponding reference factor T=-1, the y axis is inverted.

three CH<sub>3</sub> protons of an Fe–CH<sub>3</sub> fragment, with each proton having an intrinsic traceless anisotropic hyperfine tensor of arbitrary rhombicity and with its unique  $T_3$  axis tipped within its Fe–C–H plane by an arbitrary angle  $\delta$  with respect to the Fe–C rotation (z) axis. We may write the tensor components for this  $^1{\rm H}$  as

$$\mathbf{T} = [T_1, T_2, T_3 \equiv T_{\parallel}] \equiv T[-(1-\eta), -(1+\eta), 2]$$
 (1)

with T as a scaling factor that sets the strength and overall sign of the interaction and where  $\eta$  defines the rhombicity, with  $\eta=0$  corresponding to a perfectly axial tensor. As illustrated in Figure 7A, if the anisotropic term were dominated by throughspace interactions between spin on the Fe and the  $^1$ H nucleus, its unique hyperfine axis,  $T_3$ , would point closely along the Fe–H vector, with tip angle  $\delta_{\rm T}\sim 22^\circ$ ; if it were dominated by interaction with local spin on carbon, the unique axis would point along the C–H bond, with  $\delta_{\rm L}\sim 70^\circ$ .

As shown in the Supporting Information, when the methyl group rotates about the Fe-C axis rapidly enough for the three protons to yield a single, joint, averaged <sup>1</sup>H hyperfine tensor in the 2D field-frequency pattern of orientation-selective ENDOR spectra collected at fields across the EPR envelope, then this rapid rotation must have averaged the components of the site tensors to yield a single average traceless anisotropic hyperfine tensor with a common orientation, A1av, and this averaging does not depend on the nature of the motion—being the same for all types of averaging in which the potential surface for methyl rotation does not favor a particular methyl rotamer. The anisotropic contribution to this averaged tensor,  $T1^{av}$  (eq S3), is precisely axial, and is reoriented so that its unique component,  $T1_{\parallel}^{av}$ , lies along the Fe-C bond, the rotation axis, as shown in Scheme 1. Thus, the Euler angles determined from the simulation of the 2D pattern of M1-CH<sub>3</sub> <sup>1</sup>H ENDOR spectra, which describe the orientation of the axial hyperfine tensor A1<sup>av</sup> relative to the g-frame,  $\varphi = 0$ ,  $\theta = 55^{\circ}$  for M1-CH<sub>3</sub>, in fact describe the orientation of the Fe-C bond relative to the g-frame. As illustrated in Figure 8, this places  $g_{\parallel}$  nearly

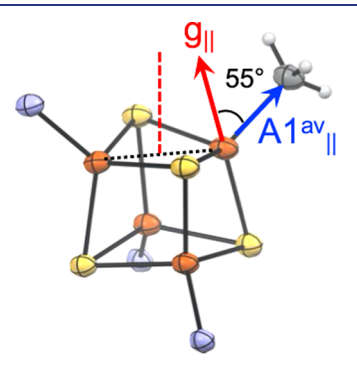


**Figure 8.** ENDOR-derived relative orientations of  $g_{\parallel}$  (red arrow) and  $A1_{\parallel}^{\text{av}}$  (blue arrow), and the resulting orientation of  $g_{\parallel}$  relative to the compression axis of the **M-CH**<sub>3</sub> [Fe<sub>4</sub>S<sub>4</sub>]<sup>3+</sup> cluster, which, as described in ref 18, is normal (dashed red line) to the face for which the Fe–Fe–CH<sub>3</sub> angle is 138°. Thermal ellipsoids (30%); orange (Fe), yellow (S), blue (N), gray (C), and white (H). Ligand is trimmed; anion and solvent are removed.

parallel to the compression axis of the M-CH $_3$  [Fe $_4$ S $_4$ ] $^{3+}$  cluster,  $^{18}$  analogous to the orientation of  $g_{\parallel}$  seen in single-crystal EPR studies of [Fe $_4$ S $_4$ ] $^{3+}$  clusters.  $^{35,36}$ 

The rotational averaging further causes the values of the observed averaged tensor components to become functions of the tip angle  $\delta$  of the site tensors relative to the Fe–C bond (Figure 7 and eq S3). As illustrated in Figure 7B, the value of the observed  $T1_{\parallel}^{\text{av}}$  drops with increasing  $\delta$ , crosses through zero at an angle  $\delta > 45^{\circ}$  that depends on  $\eta$ , then changes sign (eqs S3). The components of the averaged  $^{1}\text{H}$  anisotropic hyperfine tensor determined for M1-CH<sub>3</sub> were given above,  $T1_{\parallel}^{\text{av}} = -4.2 \text{ MHz}$ ,  $T1_{\perp}^{\text{av}} = +2.1 \text{ MHz}$ . The measured negative

value of the unique component,  $T1_{\parallel}^{\text{av}}$ , is consistent in its negative sign with assignment of the scaling factor, T (eq 1), to a through-space dipolar interaction of "down" spin on the methyl-bound Fe center with the methyl <sup>1</sup>H (Figure 7A). Given the geometry of the Fe–CH<sub>3</sub> moiety, if the intrinsic (nonaveraged) anisotropic interaction T (eq 1) is assigned to such an interaction, the intrinsic  $T_{\parallel}$  would be tipped by an angle of  $\delta_{\text{T}} \sim 22^{\circ}$  (Figure 7, left), and thus its contribution to  $T1_{\parallel}^{\text{av}}$  would retain the negative sign of the scale-parameter, T (Figure 7, right).

This assignment of the anisotropic hyperfine coupling to the through-space interaction with Fe, rather than to interaction with local spin on C, is supported by the magnitude of  $T1_{\parallel}^{av}$ , which is consistent with that expected for dipolar coupling to Fe when it is noted that eq S3 then predicts an observed averaged value,  $T1_{\parallel}^{av}/2T \sim 0.8$  (see Figure 7B). As discussed below, the combination of this decrease in the measured M1 anisotropic coupling caused by rotational averaging, plus the overall hyperfine averaging for the rotating M1 methyl, leads to the slightly smaller breadth of the M1 methyl <sup>1</sup>H ENDOR pattern compared to that for the M2 methyl.

#### ■ DISCUSSION AND CONCLUSIONS

Complex M-CH<sub>3</sub>, with its [Fe<sub>4</sub>S<sub>4</sub>]<sup>3+</sup>-CH<sub>3</sub> organometallic bond, provides a crystallographically characterized realization of the ENDOR-derived structures of the alkyl-ligated [Fe<sub>4</sub>S<sub>4</sub>]<sup>3+</sup> states of radical SAM enzymes: the  $\Omega_{\rm M}$  state, whose Fe-CH<sub>3</sub> bond precisely parallels that displayed by M-CH<sub>3</sub> (Figure 1), as well as paralleling the Fe-alkyl bond of  $\Omega$  itself, the catalytically central enzymatic intermediate in which it is the 5'-dAdo moiety that forms an Fe-C5' bond. 12 The Mössbauer and NMR studies of M-CH<sub>3</sub> established the unusual electronic structure effects imparted to the cluster by a strong field alkyl ligand, most especially the Fe<sup>3+</sup> valence localization of the alkylated iron, and thus lay the foundation for understanding the overall electronic structures of  $[Fe_4S_4]^{3+}$ -alkyl radical SAM intermediates. 18 This report has built on this foundation by probing the Fe-C bond in detail through <sup>1</sup>H and <sup>13</sup>C ENDOR measurements that can be compared directly to those in  $\Omega_{\mathrm{M}}$ and more generally, to those of  $\Omega$  itself.

As a foundation for analysis, we first note that all freezetrapped radical SAM enzymatic [Fe<sub>4</sub>S<sub>4</sub>]<sup>3+</sup>-alkyl intermediates exhibit the doublet cluster ground state with  $g_{iso} > 2$ , characteristic of an  $[Fe_4S_4]^{3+}$  cluster. Thus, the finding that M-CH<sub>3</sub>, with its [Fe<sub>4</sub>S<sub>4</sub>]<sup>3+</sup>cluster and crystallographically characterized structure, also exhibits  $g_{iso} > 2$ , confirms the EPRderived characterization of the cluster of the transient enzymatic intermediates. Second, it is of interest that M-CH<sub>3</sub> exhibits two [Fe<sub>4</sub>S<sub>4</sub>]<sup>3+</sup>-alkyl conformers with similar properties of the Fe-C bond but slightly different g-values, for work in progress indicates that the same is true for the enzymatic intermediates. The methyl group of the M1-CH3 complex rotates rapidly at 2 K, and we have clarified how this rotation creates the observed <sup>1</sup>H hyperfine tensor of a single proton associated with the rotationally averaged methyl protons, Scheme 1. Such rotation redefines the symmetry of a single-site hyperfine tensor, making the joint, averaged tensor precisely axial; it reorients this axial tensor so that the unique axis is parallel to the Fe-C bond; and it modifies the component values from those of the site tensor, as shown in Figure 7B (see eq S3).

Considering the properties of the Fe-alkyl bond itself, methyl group interactions with the "down"-spin on the unique

Fe cause both conformers of M-CH<sub>3</sub> to exhibit a small positive and essentially isotropic <sup>13</sup>C coupling constant, indicative of positive ("up") spin density induced on carbon. The magnitude of the M-CH<sub>3</sub> coupling,  $a_{iso}(^{13}C) \sim +6$  MHz, is quite comparable to that observed for  $\Omega$ ,  $|a_{iso}|^{(13)} \sim 9$  MHz,  $^{12}$ while both couplings are somewhat smaller than  $|a_{iso}(^{13}C)|$ ~18 MHz for  $\Omega_{\rm M}$ ; is notably, the coupling is more than an order of magnitude smaller than that purported for  $\Omega$  in a recent DFT study.<sup>37</sup> In contrast, the "down" spin on the unique Fe induces a negative isotropic <sup>1</sup>H hyperfine coupling to the methyl protons of both M-CH<sub>3</sub> conformers, and the magnitude of their  $a_{iso}(^{1}H)$  also compares well with the  $^{1}H$ coupling in  $\Omega$ ,  $|a_{iso}(^{1}H)| = 7$  MHz, as follows. 11 The rotationally averaged methyl hyperfine tensor of M1-CH3 has an isotropic coupling of  $a_{iso}(^{1}H) = -8.5 \text{ MHz}$  and anisotropic coupling with unique value  $T1_{\parallel}^{av} = -4.2$  MHz, while the 2D ENDOR pattern of M2-CH<sub>3</sub> (Figure S5) is satisfactorily reproduced by the sum of signals from the three tetrahedrally oriented protons of a static methyl group (Scheme 1) with <sup>1</sup>H tensors that have similar isotropic couplings,  $a_{iso}(^{1}H) \sim -(8 \leftrightarrow$ 10) MHz, and an average value for the unique component of the anisotropic coupling tensor of,  $T2_{\parallel}^{\text{av}} = -5 \text{ MHz}$ . The latter corresponds to  $T1_{\parallel}^{av}$  after taking into account the decrease in  $T1_{\parallel}^{av}$  associated with rotational averaging according to eq S3 (Figure 7B). The resulting equivalence of the intrinsic <sup>1</sup>H hyperfine tensors in the two conformers shows that the effects that slightly alter the g-values of the M-CH<sub>3</sub> conformers and modulate the dynamics of methyl group rotation nonetheless do not alter the actual Fe-CH<sub>3</sub> bonding.

<sup>13</sup>C and <sup>1</sup>H ENDOR/PESTRE hyperfine sign measurements of the enzymatic  $\Omega$  and  $\Omega_{M}$  intermediates will test whether they exhibit the same isotropic coupling signs as that of M-CH<sub>3</sub>, as well as the corresponding magnitudes; if so, this will confirm that the alkyls in the enzymatic intermediates are likewise bound to a valence-localized, spin-down Fe<sup>3+</sup>, with implications for the cluster electronic structure previously discussed. 18 Such comparisons of the properties of  $\Omega$  and  $\Omega_{
m M}$ with those of M-CH<sub>3</sub>, in combination with additional quantum computations and synthetic modeling, will address the extent to which the higher coordination number of the unique Fe in the  $\Omega$ 's, with the methionyl amino acid moiety of SAM providing additional ligand(s), affects the electronic structure of the alkylated Fe site, and thus the properties of the Fe-alkyl bond. Moreover, the hyperfine coupling values reported herein—the first measured for a crystallographically characterized [Fe<sub>4</sub>S<sub>4</sub>]<sup>3+</sup>-alkyl cluster-will help benchmark computational predictions for the hyperfine coupling in the enzymatic  $[Fe_4S_4]^{3+}$ -alkyl intermediates  $\Omega$  and  $\Omega_M$ .

#### ASSOCIATED CONTENT

#### Supporting Information

The Supporting Information is available free of charge at https://pubs.acs.org/doi/10.1021/jacs.2c07155.

Discussion of solvent dependence of EPR, extended discussion of the <sup>1</sup>H ENDOR of M-CH<sub>3</sub>, including further analysis of rotational averaging, with discussion of rotational averaging of the <sup>2</sup>H quadrupole interaction in M1-CD<sub>3</sub> (PDF)

#### AUTHOR INFORMATION

#### **Corresponding Authors**

Daniel L. M. Suess — Department of Chemistry, Massachusetts Institute of Technology, Cambridge, Massachusetts 02139, United States; orcid.org/0000-0002-0916-1973; Email: suess@mit.edu

Brian M. Hoffman — Department of Chemistry, Northwestern University, Evanston, Illinois 60208, United States; orcid.org/0000-0002-3100-0746; Email: bmh@northwestern.edu

#### **Authors**

Madeline B. Ho — Department of Chemistry, Northwestern University, Evanston, Illinois 60208, United States; orcid.org/0000-0001-6351-2132

Richard J. Jodts — Department of Chemistry, Northwestern University, Evanston, Illinois 60208, United States; orcid.org/0000-0001-7467-492X

Youngsuk Kim — Department of Chemistry, Massachusetts Institute of Technology, Cambridge, Massachusetts 02139, United States; Present Address: Department of Chemistry, Pusan National University, Busan 46241, Korea; orcid.org/0000-0002-7378-2301

Alex McSkimming — Department of Chemistry, Massachusetts Institute of Technology, Cambridge, Massachusetts 02139, United States; Present Address: Department of Chemistry, Tulane University, New Orleans, Louisiana 70118, United States; orcid.org/0000-0002-7447-9339

Complete contact information is available at: https://pubs.acs.org/10.1021/jacs.2c07155

#### **Notes**

The authors declare no competing financial interest.

#### ACKNOWLEDGMENTS

The authors acknowledge the National Science Foundation (MCB-1908587 to B.M.H.) and the National Institutes of Health (GM111097 to B.M.H. and GM136882 to D.L.M.S.) for supporting this work.

#### REFERENCES

- (1) Broderick, J. B.; Duffus, B. R.; Duschene, K. S.; Shepard, E. M. Radical S-Adenosylmethionine Enzymes. *Chem. Rev.* **2014**, *114*, 4229–4317.
- (2) Frey, P. A.; Hegeman, A. D.; Ruzicka, F. J. The Radical SAM Superfamily. Crit. Rev. Biochem. Mol. Biol. 2008, 43, 63–88.
- (3) Walsby, C. J.; Ortillo, D.; Broderick, W. E.; Broderick, J. B.; Hoffman, B. M. An Anchoring Role for FeS Clusters: Chelation of the Amino Acid Moiety of S-Adenosylmethionine to the Unique Iron Site of the [4Fe-4S] Cluster of Pyruvate Formate-Lyase Activating Enzyme. J. Am. Chem. Soc. 2002, 124, 11270–11271.
- (4) Walsby, C. J.; Hong, W.; Broderick, W. E.; Cheek, J.; Ortillo, D.; Broderick, J. B.; Hoffman, B. M. Electron-Nuclear Double Resonance Spectroscopic Evidence That S-Adenosylmethionine Binds in Contact with the Catalytically Active [4Fe–4S]<sup>+</sup> Cluster of Pyruvate Formate-Lyase Activating Enzyme. J. Am. Chem. Soc. 2002, 124, 3143–3151.
- (5) Dey, A.; Peng, Y.; Broderick, W. E.; Hedman, B.; Hodgson, K. O.; Broderick, J. B.; Solomon, E. I. S. K-Edge XAS and DFT Calculations on SAM Dependent Pyruvate Formate-Lyase Activating Enzyme: Nature of Interaction between the Fe<sub>4</sub>S<sub>4</sub> Cluster and SAM and Its Role in Reactivity. *J. Am. Chem. Soc.* **2011**, 133, 18656–18662.
- (6) Krebs, C.; Broderick, W. E.; Henshaw, T. F.; Broderick, J. B.; Huynh, B. H. Coordination of Adenosylmethionine to a Unique Iron Site of the [4Fe-4S] of Pyruvate Formate-Lyase Activating Enzyme: A

- Mössbauer Spectroscopic Study. J. Am. Chem. Soc. 2002, 124, 912–913.
- (7) Henshaw, T. F.; Cheek, J.; Broderick, J. B. The [4Fe-4S]<sup>1+</sup> Cluster of Pyruvate Formate-Lyase Activating Enzyme Generates the Glycyl Radical on Pyruvate Formate-Lyase: EPR-Detected Single Turnover. *J. Am. Chem. Soc.* **2000**, *122*, 8331–8332.
- (8) Lieder, K. W.; Booker, S.; Ruzicka, F. J.; Beinert, H.; Reed, G. H.; Frey, P. A. S-Adenosylmethionine-Dependent Reduction of Lysine 2,3-Aminomutase and Observation of the Catalytically Functional Iron-Sulfur Centers by Electron Paramagnetic Resonance. *Biochemistry* 1998, 37, 2578–2585.
- (9) Frey, P. A.; Magnusson, O. T. S-Adenosylmethionine: A Wolf in Sheep's Clothing, or a Rich Man's Adenosylcobalamin? *Chem. Rev.* **2003**, *103*, 2129–2148.
- (10) Moss, M.; Frey, P. A. The Role of S-Adenosylmethionine in the Lysine 2,3-Aminomutase Reaction. *J. Biol. Chem.* **1987**, 262, 14859—14862
- (11) Byer, A. S.; Yang, H.; McDaniel, E. C.; Kathiresan, V.; Impano, S.; Pagnier, A.; Watts, H.; Denler, C.; Vagstad, A. L.; Piel, J.; Duschene, K. S.; Shepard, E. M.; Shields, T. P.; Scott, L. G.; Lilla, E. A.; Yokoyama, K.; Broderick, W. E.; Hoffman, B. M.; Broderick, J. B. Paradigm Shift for Radical S-Adenosyl-L-Methionine Reactions: The Organometallic Intermediate  $\Omega$  Is Central to Catalysis. *J. Am. Chem. Soc.* 2018, 140, 8634–8638.
- (12) Horitani, M.; Shisler, K.; Broderick, W. E.; Hutcheson, R. U.; Duschene, K. S.; Marts, A. R.; Hoffman, B. M.; Broderick, J. B. Radical SAM Catalysis Via an Organometallic Intermediate with an Fe-[5'-C]-Deoxyadenosyl Bond. *Science* **2016**, 352, 822–825.
- (13) Lundahl, M. N.; Sarksian, R.; Yang, H.; Jodts, R. J.; Pagnier, A.; Smith, D. F.; Mosquera, M. A.; van der Donk, W. A.; Hoffman, B. M.; Broderick, W. E.; Broderick, J. B. Mechanism of Radical S-Adenosyl-L-Methionine Adenosylation: Radical Intermediates and the Catalytic Competence of the 5'-Deoxyadenosyl Radical. *J. Am. Chem. Soc.* 2022, 144, 5087–5098.
- (14) Balo, A. R.; Caruso, A.; Tao, L.; Tantillo, D. J.; Seyedsayamdost, M. R.; Britt, R. D. Trapping a Cross-Linked Lysine-Tryptophan Radical in the Catalytic Cycle of the Radical SAM Enzyme SuiB. *Proc. Natl. Acad. Sci. U.S.A.* **2021**, *118*, No. e2101571118.
- (15) Yang, H.; Impano, S.; Shepard, E. M.; James, C. D.; Broderick, W. E.; Broderick, J. B.; Hoffman, B. M. Photoinduced Electron Transfer in a Radical SAM Enzyme Generates an S-Adenosylmethionine Derived Methyl Radical. *J. Am. Chem. Soc.* **2019**, *141*, 16117–16124.
- (16) Ye, M.; Thompson, N. B.; Brown, A. C.; Suess, D. L. M. A Synthetic Model of Enzymatic  $[Fe_4S_4]$ —Alkyl Intermediates. *J. Am. Chem. Soc.* **2019**, *141*, 13330–13335.
- (17) Brown, A. C.; Suess, D. L. M. Reversible Formation of Alkyl Radicals at  $[Fe_4S_4]$  Clusters and Its Implications for Selectivity in Radical SAM Enzymes. *J. Am. Chem. Soc.* **2020**, *142*, 14240–14248.
- (18) McSkimming, A.; Sridharan, A.; Thompson, N. B.; Müller, P.; Suess, D. L. M. An [Fe<sub>4</sub>S<sub>4</sub>]<sup>3+</sup>–Alkyl Cluster Stabilized by an Expanded Scorpionate Ligand. *J. Am. Chem. Soc.* **2020**, *142*, 14314–14323.
- (19) Werst, M. M.; Davoust, C. E.; Hoffman, B. M. Ligand Spin Densities in Blue Copper Proteins by Q-Band <sup>1</sup>H and <sup>14</sup>N ENDOR Spectroscopy. *J. Am. Chem. Soc.* **1991**, *113*, 1533–1538.
- (20) Davoust, C. E.; Doan, P. E.; Hoffman, B. M. Q-Band Pulsed Electron Spin-Echo Spectrometer and Its Application to ENDOR and ESEEM. *J. Magn. Reson., Ser. A* **1996**, *119*, 38–44.
- (21) Stoll, S.; Schweiger, A. Easyspin, a Comprehensive Software Package for Spectral Simulation and Analysis in EPR. *J. Magn. Reson.* **2006**, *178*, 42–55.
- (22) Doan, P. E. Combining Steady-State and Dynamic Methods for Determining Absolute Signs of Hyperfine Interactions: Pulsed ENDOR Saturation and Recovery (PESTRE). *J. Magn. Reson.* **2011**, 208, 76–86.
- (23) Cutsail, G. E., 3rd; Telser, J.; Hoffman, B. M. Advanced Paramagnetic Resonance Spectroscopies of Iron-Sulfur Proteins:

Electron Nuclear Double Resonance (ENDOR) and Electron Spin Echo Envelope Modulation (ESEEM). Biochim. Biophys. Acta 2015, 1853, 1370-1394.

- (24) Clough, S.; Poldy, F. Study of Tunneling Rotation of Methyl Groups by Electron Spin Resonance and Electron Nuclear Double Resonance. J. Chem. Phys. 1969, 51, 2076-2084.
- (25) Kubota, S.; Iwaizumi, M.; Ikegami, Y.; Shimokoshi, K. Anisotropic Hyperfine Interaction in the Electron Spin Resonance Spectrum of the Methyl Radical Trapped in CH<sub>3</sub>COONa·3D<sub>2</sub>O Crystal at Low Temperatures. J. Chem. Phys. 1979, 71, 4771-4776.
- (26) Kirste, B.; Van Willigen, H. ENDOR Study of Bis-(Acetylacetonato)Copper(II) in Solid Solution. J. Phys. Chem. A **1983**, 87, 781-788.
- (27) Sharples, K. M.; Carter, E.; Hughes, C. E.; Harris, K. D. M.; Platts, J. A.; Murphy, D. M. An ENDOR and DFT Analysis of Hindered Methyl Group Rotations in Frozen Solutions of Bis-(Acetylacetonato)-Copper(II). Phys. Chem. Chem. Phys. 2013, 15, 15214-15222.
- (28) DeRose, V. J.; Hoffman, B. M. Protein Structure and Mechanism Studied by Electron Nuclear Double Resonance Spectroscopy. In Methods in Enzymology Sauer, K., Ed.; Academic Press: New York, 1995; Vol. 246, pp 554-589.
- (29) Hoffman, B. M.; DeRose, V. J.; Doan, P. E.; Gurbiel, R. J.; Houseman, A. L. P.; Telser, J. Metalloenzyme Active-Site Structure and Function through Multifrequency CW and Pulsed ENDOR. Biol. Magn. Reson. 1993, 13, 151-218.
- (30) Lee, Y.; Kinney, R. A.; Hoffman, B. M.; Peters, J. C. A Nonclassical Dihydrogen Adduct of S = 1/2 Fe(I). J. Am. Chem. Soc. 2011, 133, 16366-16369.
- (31) Gunderson, W. A.; Suess, D. L.; Fong, H.; Wang, X.; Hoffmann, C. M.; Cutsail, G. E., III; Peters, J. C.; Hoffman, B. M. Free H<sub>2</sub> Rotation vs Jahn-Teller Constraints in the Nonclassical Trigonal (TPB)Co-H<sub>2</sub> Complex. J. Am. Chem. Soc. 2014, 136, 14998-15009.
- (32) Freed, J. H. Quantum Effects of Methyl-Group Rotations in Magnetic Resonance: ESR Splittings and Linewidths. J. Chem. Phys. **1965**, 43, 1710-1720.
- (33) Geoffroy, M.; Kispert, L. D.; Hwang, J. S. An ESR, ENDOR, and ELDOR Study of Tunneling Rotation of a Hindered Methyl Group in X-Irradiated 2,2,5-Trimethyl-1,3-Dioxane-4,6-Dione Crystals. J. Chem. Phys. 1979, 70, 4238-4242.
- (34) Brosi, R.; Illarionov, B.; Mathes, T.; Fischer, M.; Joshi, M.; Bacher, A.; Hegemann, P.; Bittl, R.; Weber, S.; Schleicher, E. Hindered Rotation of a Cofactor Methyl Group as a Probe for Protein-Cofactor Interaction. J. Am. Chem. Soc. 2010, 132, 8935-
- (35) Gloux, J.; Gloux, P.; Lamotte, B.; Mouesca, J.-M.; Rius, G. The Different [Fe<sub>4</sub>S<sub>4</sub>]<sup>3+</sup> and [Fe<sub>4</sub>S<sub>4</sub>]<sup>+</sup> Species Created By Gamma Irradiation in Single Crystals of the (Et<sub>4</sub>N)<sub>2</sub>[Fe<sub>4</sub>S<sub>4</sub>(SBenz)<sub>4</sub>] Model Compound: Their EPR Description and Their Biological Significance. J. Am. Chem. Soc. 1994, 116, 1953-1961.
- (36) Rius, G.; Lamotte, B. Single-Crystal Endor Study of a 57Fe-Enriched Iron-Sulfur [Fe<sub>4</sub>S<sub>4</sub>]<sup>3+</sup> Cluster. J. Am. Chem. Soc. 1989, 111, 2464-2469.
- (37) Donnan, P. H.; Mansoorabadi, S. O. Broken-Symmetry Density Functional Theory Analysis of the  $\Omega$  Intermediate in Radical S-Adenosyl-L-Methionine Enzymes: Evidence for a Near-Attack Conformer over an Organometallic Species. J. Am. Chem. Soc. 2022, 144, 3381-3385.

## **□** Recommended by ACS

#### Computational Description of Alkylated Iron-Sulfur **Organometallic Clusters**

Richard J. Jodts, Martín A. Mosquera, et al.

JUNE 12, 2023

JOURNAL OF THE AMERICAN CHEMICAL SOCIETY

RFAD 🗹

#### **Evidence of Atypical Structural Flexibility of the Active Site** Surrounding of an [FeFe] Hydrogenase from Clostridium beijerinkii

Patrick S. Corrigan, Alexey Silakov, et al.

MAY 10, 2023

JOURNAL OF THE AMERICAN CHEMICAL SOCIETY

READ **C** 

#### **Direct Cysteine Desulfurase Activity Determination by NMR** and the Study of the Functional Role of Key Structural **Elements of Human NFS1**

Karl E. Sewell, Javier Santos, et al.

JULY 06, 2023

ACS CHEMICAL BIOLOGY

READ 🗹

#### Enzymatic Hydroxylation of Aliphatic C-H Bonds by a Mn/Fe Cofactor

Magan M. Powell, Jonathan Rittle, et al.

JULY 20, 2023

JOURNAL OF THE AMERICAN CHEMICAL SOCIETY

RFAD 🗹

Get More Suggestions >